

Challenges to magnetic doping of thin films of the Dirac semimetal Cd_3As_2

Run Xiao,¹ Jacob T Held,² Jeffrey Rable,¹ Supriya Ghosh,²
Ke Wang,³ K. Andre Mkhoyan,² and Nitin Samarth^{1,*}

¹*Department of Physics, The Pennsylvania State
University, University Park, PA 16802, USA*

²*Department of Chemical Engineering and Materials Science,
University of Minnesota, Minneapolis, MN 55455, USA*

³*Materials Research Institute, The Pennsylvania State University, University Park PA 16802*

(Dated: December 23, 2021)

Abstract

Magnetic doping of topological quantum materials provides an attractive route for studying the effects of time-reversal symmetry breaking. Thus motivated, we explore the introduction of the transition metal Mn into thin films of the Dirac semimetal Cd_3As_2 during growth by molecular beam epitaxy. Scanning transmission electron microscopy measurements show the formation of a Mn-rich phase at the top surface of Mn-doped Cd_3As_2 thin films grown using both uniform doping and delta doping. This suggests that Mn acts as a surfactant during epitaxial growth of Cd_3As_2 , resulting in phase separation. Magnetometry measurements of such samples indicate a ferromagnetic phase with out-of-plane magnetic anisotropy. Electrical magneto-transport measurements of these films as a function of temperature, magnetic field, and chemical potential reveal a lower carrier density and higher electron mobility compared to pristine Cd_3As_2 films grown under similar conditions. This suggests that the surfactant effect might also serve to getter impurities. We observe robust quantum transport (Shubnikov-de Haas oscillations and an incipient integer quantum Hall effect) in very thin (7 nm) Cd_3As_2 films despite being in direct contact with a structurally disordered surface ferromagnetic overlayer.

I. INTRODUCTION

Magnetic doping of quantum materials such as semiconductors and topological insulators (TIs) is a well established route to the discovery of interesting emergent quantum phenomena.[1–5] Magnetically-doped semiconductors such as (Ga,Mn)As have provided an important platform for proof-of-concept spintronic devices [6] while magnetic doping of certain TIs has led to the discovery of the quantum anomalous Hall effect [7–9]. In the latter case, the key physics is driven by the breaking of time-reversal symmetry by ferromagnetic order induced by the exchange interaction between transition metal dopants (Cr, V, Mn, and Fe) and the extended band states of the TI in the $(\text{Bi,Sb})_2(\text{Te,Se})_3$ family.

The success of transition metal doping of semiconductors and TIs provides a strong motivation for exploring similar magnetic doping of other topological materials such as topological Dirac semimetals [10–15]. Topological Dirac semimetals host three-dimensional Dirac fermions and can be identified as a parent phase of other topological phases, for

* Corresponding author: nsamarth@psu.edu

instance, Weyl semimetals [16, 17]. Introducing magnetic dopants into a Dirac semimetal to break the time-reversal symmetry could lead to the degenerate Dirac fermions separating into two (or four) Weyl fermions and a Weyl semimetal phase [19].

In the last decade, Cd_3As_2 has been theoretically predicted [18] and experimentally demonstrated [12–14] as a Dirac semimetal. More recently, high-quality Cd_3As_2 thin films have been successfully grown using molecular beam epitaxy (MBE) [20–23] and exhibit the quantum Hall effect [21, 24, 25]. The past success of MBE growth of magnetically-doped semiconductors provides a strong motivation to explore magnetic doping of MBE-grown Cd_3As_2 thin films as a route toward breaking time-reversal symmetry [19] for realizing novel topological phases such as magnetic Weyl semimetals [26–28] and monopole superconductors [29]. We are aware of only two published reports on magnetic doping of Cd_3As_2 thin films using Cr [30] and Mn [31]. These studies principally relied on electrical magnetoresistance measurements to draw conclusions about the effect of magnetic dopants on the Dirac semimetal states and assumed that the magnetic dopants were homogeneously distributed throughout the Cd_3As_2 film.

In this paper, we describe our attempts to use MBE to dope Mn into the Dirac semimetal Cd_3As_2 . We present a systematic structural and magnetic study of heterostructures using high-angle annular dark-field scanning transmission electron microscopy (HAADF-STEM), energy dispersive X-ray spectroscopy (EDX), atomic force microscopy (AFM), high-resolution x-ray diffraction (XRD), superconducting quantum interference device (SQUID) magnetometry, and electrical transport. We find that instead of being incorporated into the Cd_3As_2 lattice, the Mn dopants form a Mn-rich layer on the top of the Cd_3As_2 layer. The Mn-rich layer shows insulating behavior and lowers the carrier density in the Cd_3As_2 layer underneath. Remarkably, even though the Mn-rich phase/ Cd_3As_2 heterostructure exhibits ferromagnetism at room temperature with out-of-plane anisotropy, the samples show pronounced quantum oscillations and an incipient integer quantum Hall effect at low temperature.

II. RESULTS AND DISCUSSION

The Mn-doped Cd_3As_2 thin films were grown by MBE in a Veeco EPI 930 chamber. We used epi-ready miscut semi-insulating GaAs (111)B substrates (1° toward $(2\bar{1}\bar{1})$). Elemental

source materials were evaporated from standard effusion cells containing As (99.999995%), Ga(99.99999%), Sb(99.9999%), Cd (99.9999%), and Mn (99.9998%). The epi-ready GaAs substrates were first annealed inside the MBE chamber to flash off the native oxide at a thermocouple temperature of 720 °C (the actual temperature is likely 580 °C). Then, we deposited a thin ($\sim 2\text{nm}$) GaAs layer at the same substrate temperature to smooth the surface. Subsequently, the substrates were cooled down to 480°C under As_4 flux for the growth of the GaSb buffer layer with an Sb/Ga beam equivalent pressure (BEP) ratio of 7. We note that the both the GaAs and GaSb layers are highly insulating, as confirmed by control measurements. The substrates were then cooled down to 400 °C under Sb_4 flux, and further cooled down to 180 °C after closing the Sb shutter for the growth of Mn-doped Cd_3As_2 . Once the sample temperature was stable at 180 °C, we used the Cd, As, and Mn effusion cells with BEP of Cd around 6×10^{-8} Torr, As around 2×10^{-8} Torr and Mn around 1.2×10^{-9} Torr.

We attempted to grow Mn-doped Cd_3As_2 thin films using two methods: uniform doping wherein the Mn flux is constant during the growth of Cd_3As_2 and the delta doping method wherein we interrupt the growth of Cd_3As_2 and deposit a fractional monolayer of MnAs. The latter approach has been effective in magnetic doping of II-VI and III-V semiconductors [32, 33]. Both growth methods resulted in films with similar characteristics. Reflection high-energy electron diffraction (RHEED) measurements during the growth showed streaky patterns in either approach, indicating a relatively flat surface with some disorder even when depositing a Mn-rich layer (Fig. 1(a)). Post-growth, we carried out *ex situ* AFM measurements (Fig. 1(b)) that indicated a root mean square surface roughness of 1.77 nm over an area of $10 \times 10 \mu\text{m}^2$. The steps in the AFM image are due to the miscut substrate; these help prevent twinning defects and improve the quality of the sample. The $1 \times 1 \mu\text{m}^2$ AFM image in Fig. 1(b) shows the atomic steps of the heterostructure, indicative of the epitaxial growth of the heterostructure. Figure 1(c) compares the XRD scan of a nominally uniformly Mn-doped Cd_3As_2 film of nominal 25 nm thickness; the plot compares this XRD scan with that of a pristine Cd_3As_2 film. We observe extra diffraction peaks in the Mn-doped film suggesting the presence of an extra phase. However, from the XRD scan alone, we are unable to identify the crystal structure of this phase.

To understand the crystalline structure and elemental distribution within the heterostructures, we used cross-sectional HAADF-STEM imaging and STEM-EDX elemental mapping.

We prepared TEM lamella for STEM analysis on a FEI Helios Nanolab G4 dual-beam Focused Ion Beam (FIB). Amorphous carbon was first deposited on the films to protect the surface from damage due to exposure to the ion beam. STEM imaging and EDX spectroscopy were performed on an aberration-corrected FEI Titan G2 60-300 (S)TEM microscope equipped with a CEOS DCOR probe corrector and a super-X EDX spectrometer. The microscope was operated at 300 keV. We acquired HAADF-STEM images with a probe convergence semi-angle of 25.5 mrad and detector inner and outer collection angles of 55 and 200 mrad respectively. We now discuss the TEM measurements obtained from a uniformly Mn-doped Cd_3As_2 film of nominal 15 nm thickness. Measurements taken on a delta-doped film of similar thickness yield qualitatively similar results (see Supplementary Material at xxx).

High magnification HAADF-STEM images of the film cross-section revealed a crystalline Mn- Cd_3As_2 film of thickness ~ 13 nm, epitaxial to the GaSb substrate (Fig. 2(a)). A uniform amorphous-like layer (~ 5 nm thick) of darker contrast is seen on top of the film. STEM-EDX elemental mapping, shown in Fig. 2(a), was used to obtain compositional information from the heterostructure. Surprisingly, instead of incorporating Mn throughout the film, the growth procedure, illustrated in Fig. 2(b), produced a segregated Mn-rich phase at the top surface of the Cd_3As_2 film. The resultant structure is visible in the EDX maps and illustrated in Fig. 2(c).

Averaging the results from several STEM-EDX data sets revealed that the darker contrast region seen in STEM images on top of the Cd_3As_2 film is primarily composed of a Mn-oxide phase with small traces of Cd and As (O: 49 at%, Mn: 39 at%; Cd and As: 12 at%). While most of the Mn migrated to the surface, EDX analysis revealed < 5 at% Mn content in the Cd_3As_2 film layer, indicating some doping of the films with Mn. In addition to the uniform Mn-rich layer, some regions exhibited islands rising out of the film surface with more mixing between the Mn, Cd and As (Cd: 17.3 at%, Mn: 27.4 at%, O: 24.5 at%, As: 29.8 at%). These islands were mostly amorphous with some crystalline regions closer to the surface of the film. The phase separation seen from the STEM-EDX data is supported by the low solubility of Mn in Cd_3As_2 . As a result, even for the MBE growth under non-equilibrium conditions, it is hard to overcome the kinetic barrier to form Mn-doped Cd_3As_2 [34].

Since our attempt to introduce magnetic dopants into Cd_3As_2 thin films inadvertently resulted in a phase-segregated heterostructure wherein a Mn-rich compound is cleanly in-

terfaced with a Cd_3As_2 film, two important questions arise. First, is the Mn-rich phase magnetically ordered? If so, how does its presence affect the electronic transport properties of the Cd_3As_2 film with which it is directly interfaced? Naively, one might anticipate that interfacial exchange interaction between the magnetic moments in the overlayer and the band electrons in the Cd_3As_2 film would result in a degradation of the mobility due to spin-dependent scattering. We now address the magnetic and electrical transport properties of these Mn-doped Cd_3As_2 films. Since we have established that the actual sample structure consists of a thin Mn-rich overlayer interfaced with a Cd_3As_2 film regardless of the growth method used, we will refer to the samples being measured as heterostructures with x nm Mn-rich layer/ y nm Cd_3As_2 .

We first discuss SQUID magnetometry measurements of a 1 nm Mn-rich layer/ 7 nm Cd_3As_2 heterostructure that results from the delta-doping method with 6 repeats of (sub-monolayer MnAs/1.25 nm Cd_3As_2); the thicknesses in the final structure are estimated from HAADF-STEM measurements of a thicker sample using similar conditions with twice the thickness. The measurements were carried out in a Quantum Design SQUID magnetometer with the sample mounted in a straw for field parallel to and field normal to the sample plane. Figure 3 (a) shows the magnetization (M) versus field (H) at $T = 10$ K for this sample with the field in plane and out-of-plane. A diamagnetic background has been subtracted in these plots. Zoomed in views of M vs. H for field in-plane (Fig. 3(b)) and out-of-plane (Fig. 3(c)) show hysteresis loops with a very large coercive field (~ 80 mT) in the former case and much smaller coercive field (~ 10 mT) in the latter. The behavior of the coercive field and the saturation field for the two field orientations are consistent with ferromagnetism in the sample with a strong out-of-plane magnetocrystalline anisotropy. This could arise from an inhomogeneous distribution of Mn forming complex nanoscale cluster phases with the other elements present in the TEM analysis (primarily O, but also containing Cd and As). We note that the most commonly known compounds involving Mn and O (MnO and Mn_3O_4) are antiferromagnetic and ferromagnetic, respectively. A more detailed understanding of the origin of ferromagnetism in such samples will require measurements such as x-ray magnetic circular dichroism and polarized neutron reflectometry.

Next, we discuss electrical transport in this 1 nm Mn-rich layer/ 7 nm Cd_3As_2 heterostructure. We fabricated the samples into $40 \mu\text{m} \times 10 \mu\text{m}$ Hall bar devices using photolithography and Ar^+ plasma dry etching. The top gate was defined by a 30 nm Al_2O_3 dielectric layer

and Ti(5 nm)/Au(50 nm) contacts deposited by atomic layer deposition and electron beam evaporation, respectively. Magnetoresistance (MR) and Hall effect measurements were carried out in a Quantum Design Physical Properties Measurement System over a temperature range $2 \text{ K} \leq T \leq 300 \text{ K}$ and in magnetic fields up to $B = 9 \text{ T}$. All the MR and Hall effect data shown have been properly field symmetrized or anti-symmetrized, respectively. Figure 3(d) shows the results of such measurements at $T = 2 \text{ K}$. Surprisingly, despite the presence of the ferromagnetic overlayer in direct contact with the Cd_3As_2 film, we observe pronounced quantum oscillations and even an incipient quantum Hall effect indicated by a Hall resistance plateau corresponding to $\rho_{xy} = \frac{1}{6} \frac{h}{e^2} = 4.3 \text{ k}\Omega$. We searched for possible signatures of an exchange coupling between the electrons in the Cd_3As_2 layer and Mn moments in the overlayer. Since the easy axis of the Mn-rich layer is out-of-plane according to our SQUID measurements, an exchange coupling between carriers in Cd_3As_2 and the Mn moments should lead to hysteresis in the field dependence of the Hall resistance and also to the MR from modifications to the quantum corrections to diffusive transport. Figure 3 (e) shows a careful sweep of the longitudinal MR and the Hall effect in the field range $-0.1 \text{ T} \leq B \leq 0.1 \text{ T}$. The low field MR shows a non-monotonic dependence on magnetic field with an initial positive MR followed by a sudden change to a negative MR at a field close to the coercive field observed in SQUID magnetometry. The negative MR at fields higher than the saturation field of the ferromagnetic layer may indicate a reduction in spin-dependent scattering. In contrast, pristine Cd_3As_2 films grown under similar conditions only show a positive MR for field perpendicular to the sample plane (see Supplementary material at xxx). We do not see any obvious signs of hysteretic or non-linear Hall resistance. It is possible that with the step size used in the magneto-transport measurements (0.01 T), we might not be able to resolve these differences given how quickly the magnetization saturates with field along the anisotropy axis and the narrowness of hysteresis loop.

To further understand the effect of the Mn-rich overlayer on quantum transport, we analyzed the quantum oscillations in the heterostructure and compared the behavior with similar measurements in pure Cd_3As_2 thin films. For the 1 nm Mn-rich layer/ 7 nm Cd_3As_2 heterostructure, the amplitude of quantum oscillations gradually decreased with increasing temperature but remained finite up to about $T = 100 \text{ K}$ as shown in Fig.4(a). We note that the $\nu = 6$ quantum Hall plateau mentioned earlier was observable up to $T = 20 \text{ K}$ in Fig. 4(b). To extract the carrier density, mobility, and effective mass of the carriers

involved in quantum transport, we studied the temperature dependence of the quantum oscillations (Figs. 4(c) and 4(d)). The carrier density and mobility were calculated using both the Drude model and quantum oscillations. Using the Drude model, we find a carrier density $n = 9.5 \times 10^{11} \text{cm}^{-2}$ and a mobility $\mu = 9200 \text{ cm}^2/\text{V/s}$ at $T = 2 \text{ K}$. The analysis of quantum oscillations yields $n = 7.2 \times 10^{11} \text{cm}^{-2}$ and $\mu = 12000 \text{ cm}^2/\text{V/s}$. The higher carrier density and lower carrier mobility deduced from Drude analysis compared to that obtained from quantum oscillations indicates the presence of low-mobility carriers that do not contribute to the quantum oscillations. The band origin of the low mobility carriers is not clear at this stage. By fitting the amplitude of the quantum oscillations using the standard Lifshitz-Kosevich formula [21], we extracted an effective mass $m^* = 0.04m_e$. This light effective mass is due to the Dirac dispersion and is in good agreement with previous studies of Cd_3As_2 thin films [21, 24, 35].

Figure 4(c) also shows the carrier density and the mobility of a pure 7 nm Cd_3As_2 thin film (at $T = 2\text{K}$) calculated from the Drude model; this film was grown under nominally identical conditions (substrate temperature and Cd:As flux ratio) to those used for the growth of Mn-delta-doped samples. The carrier density in the pure film is about 20% higher and the Drude mobility is about 50% lower than in the Mn-doped film. Our findings suggest that the Mn-rich layer does not contribute to the transport signal and perhaps passivates the Cd_3As_2 layers underneath from electronegative OH-surface adsorbates [36].

Although the Mn-rich layer lies between the Cd_3As_2 layer and the top gate, it does not appear to affect the efficiency of the top gate. As shown in Fig. 4(e) and 4(f), the chemical potential of the heterostructure can be tuned from n-type to p-type by applying a top gate voltage. The quantum oscillations are only observed in the positive gate voltage regime, indicating the higher mobility of n-type carriers. We also note that the emerging quantum Hall plateaus are observable only around zero gate voltage, which is close to the Dirac point of the Cd_3As_2 layer. Away from the Dirac point, the quantum Hall plateaus disappear because of the high carrier density in the n-type regime and the low mobility in the p-type regime.

We now discuss our results in the context of prior studies of pristine (non-magnetic) Cd_3As_2 thin films, in particular those grown on (111) GaSb/GaAs. The integer quantum Hall effect was initially observed in a (112)-oriented Cd_3As_2 thin film of 20 nm thickness [24], followed by observations in similarly grown films whose thicknesses ranged from 10 nm - 60

nm [25]. While it is clear that the integer quantum Hall effect in these Cd_3As_2 films indicates quantum transport in a two-dimensional (2D) electron gas, a complete understanding of its origin is still lacking. A systematic study of the thickness-dependence of the quantum transport appears to rule out the role of Weyl orbits in the experimentally observed quantum Hall effect. [25] This hypothesis is consistent with our observation of an incipient integer quantum Hall effect in an even thinner (7 nm) Cd_3As_2 film than in these earlier studies; in addition, we observe the quantum Hall effect in the presence of a highly structurally disordered ferromagnetic interface at the top surface. We note that recent density functional theory calculations indicate that surface Fermi arcs likely survive in Cd_3As_2 films down to the thicknesses studied experimentally here. [37] However, these Fermi arc states on the top surface would presumably not survive in the presence of the disordered magnetic layer, especially with an out-of-plane magnetization. Our results appear to suggest that the wave function of the 2D electron system in ultrathin Cd_3As_2 films, likely built from Fermi arc states and quantum confined bulk states, has a maximum located away from the top and bottom surfaces, thus being immune to perturbation by the magnetism on the top surface. At this stage, however, we do not have a rigorous calculation to support this speculation.

III. SUMMARY

In summary, we have shown that conventional magnetic doping approaches to introducing ferromagnetism into Cd_3As_2 by MBE result in a phase separation with a Mn-rich near-surface layer capping a pristine Cd_3As_2 film since Mn likely acts as surfactant. The Mn-rich region shows out-of-plane magnetic anisotropy in SQUID measurements. Surprisingly, this ferromagnetic Mn-rich layer does not negatively affect the quantum transport in the Cd_3As_2 underneath. On the contrary, compared with pure Cd_3As_2 thin films grown under identical conditions, the presence of the Mn surfactant lowers the carrier density so that the chemical potential is close to the Dirac point and leads to an enhanced electron mobility. The resulting 1 nm Mn-rich layer/ 7 nm Cd_3As_2 films show an emergent quantum Hall effect in transport measurements. This should become more robust if the samples are measured at lower temperature and at higher magnetic fields. Measurements at dilution fridge temperatures may also reveal emergent physics resulting from the presence of the ferromagnetic overlayer. Although it is hard to dope Mn directly into Cd_3As_2 using MBE, it is worthwhile using other

techniques such as polarized-neutron reflectometry to search for magnetic proximity effects of the easy-plane ferromagnetism on the Cd_3As_2 underneath. Our study indicates that extreme caution is called for in relying on magnetotransport data alone as a sign of broken time-reversal symmetry in magnetically-doped Cd_3As_2 films, especially in the absence of electron microscopy data [30].

ACKNOWLEDGMENTS

This project was supported by the Institute for Quantum Matter under DOE EFRC grant DE-SC0019331 (RX,NS). The magnetometry measurements were supported by a grant from the University of Chicago (JR,NS). The electron microscopy effort (JH,AM) was supported by SMART, one of seven centers of nCORE, a Semiconductor Research Corporation program, sponsored by the National Institute of Standards and Technology (NIST) and by the College of Science and Engineering Characterization Facility, University of Minnesota, which has received capital equipment funding from the National Science Foundation through the UMN MRSEC under Award Number DMR-2011401. We thank Chris Leighton, Paul Crowell, Yi Li, and Junyi Zhang for useful comments.

-
- [1] A. H. Macdonald, P. Schiffer, and N. Samarth, Ferromagnetic semiconductors: Moving beyond (Ga,Mn)As, *Nat. Mater.* **4**, 195 (2005).
 - [2] C.-X. Liu, X.-L. Qi, X. Dai, Z. Fang, and S.-C. Zhang, Quantum anomalous Hall effect in $\text{Hg}_{1-y}\text{Mn}_y\text{Te}$ quantum wells, *Phys. Rev. Lett.* **101**, 146802 (2008).
 - [3] R. Yu, W. Zhang, H.-J. Zhang, S.-C. Zhang, X. Dai, and Z. Fang, Quantized anomalous Hall effect in magnetic topological insulators, *Science* **329**, 61 (2010).
 - [4] S.-Y. Xu, M. Neupane, C. Liu, D. Zhang, A. Richardella, L. A. Wray, N. Alidoust, M. Leandersson, T. Balasubramanian, J. Sánchez-Barriga, O. Rader, G. Landolt, B. Slomski, J. H. Dil, J. Osterwalder, T.-R. Chang, H.-T. Jeng, H. Lin, A. Bansil, N. Samarth, and M. Z. Hasan, Hedgehog spin texture and Berry's phase tuning in a magnetic topological insulator, *Nat. Phys.* **8**, 616 (2012).

- [5] C.-Z. Chang, J. Zhang, M. Liu, Z. Zhang, X. Feng, K. Li, L.-L. Wang, X. Chen, X. Dai, Z. Fang, X.-L. Qi, S.-C. Zhang, Y. Wang, K. He, X.-C. Ma, and Q.-K. Xue, Thin films of magnetically doped topological insulator with carrier-independent long-range ferromagnetic order, *Adv. Mater.* **25**, 1065 (2013).
- [6] T. Dietl and H. Ohno, Dilute ferromagnetic semiconductors: physics and spintronic structures, *Rev. Mod. Phys.* **86**, 187 (2014).
- [7] C.-Z. Chang, J. Zhang, X. Feng, J. Shen, Z. Zhang, M. Guo, K. Li, Y. Ou, P. Wei, L.-L. Wang, Z.-Q. Ji, Y. Feng, S. Ji, X. Chen, J. Jia, X. Dai, Z. Fang, S.-C. Zhang, K. He, Y. Wang, L. Lu, X.-C. Ma, and Q.-K. Xue, Experimental observation of the Quantum anomalous Hall effect in a magnetic topological insulator, *Science* **340**, 167 (2013).
- [8] A. Kandala, A. Richardella, S. Kempinger, C.-X. Liu, and N. Samarth, Giant anisotropic magnetoresistance in a quantum anomalous Hall insulator, *Nat. Commun.* **6**, 1 (2015).
- [9] C.-Z. Chang, W. Zhao, D. Y. Kim, H. Zhang, B. A. Assaf, D. Heiman, S.-C. Zhang, C.-x. Liu, M. H. W. Chan, and J. S. Moodera, High-precision realization of robust quantum anomalous Hall state in a hard ferromagnetic topological insulator, *Nat. Mater.* **14**, 473 (2015).
- [10] Z. K. Liu, B. Zhou, Y. Zhang, Z. J. Wang, H. M. Weng, D. Prabhakaran, S.-K. Mo, Z. X. Shen, Z. Fang, X. Dai, Z. Hussain, and Y. L. Chen, Discovery of a three-dimensional topological Dirac semimetal, Na₃Bi, *Science* **343**, 864 (2014).
- [11] S.-Y. Xu, C. Liu, S. K. Kushwaha, R. Sankar, J. W. Krizan, I. Belopolski, M. Neupane, G. Bian, N. Alidoust, T.-R. Chang, H.-T. Jeng, C.-Y. Huang, W.-F. Tsai, H. Lin, P. P. Shibayev, F.-C. Chou, R. J. Cava, and M. Z. Hasan, Observation of Fermi arc surface states in a topological metal, *Science* **347**, 294 (2015).
- [12] Z. K. Liu, J. Jiang, B. Zhou, Z. J. Wang, Y. Zhang, H. Weng, D. Prabhakaran, S. K. Mo, H. Peng, P. Dudin, T. Kim, M. Hoesch, Z. Fang, X. Dai, Z. X. Shen, D. L. Feng, H. Z., and Y. L. Chen, A stable three-dimensional topological Dirac semimetal Cd₃As₂, *Nat. Mater.* **13**, 677 (2014).
- [13] M. Neupane, S.-Y. Xu, R. Sankar, N. Alidoust, G. Bian, C. Liu, I. Belopolski, T.-R. Chang, H.-T. Jeng, H. Lin, A. Bansil, F. Chou, and M. Z. Hasan, Observation of a three-dimensional topological Dirac semimetal phase in high-mobility Cd₃As₂, *Nat. Commun.* **5**, 1 (2014).
- [14] H. Yi, Z. Wang, C. Chen, Y. Shi, Y. Feng, A. Liang, Z. Xie, S. He, J. He, Y. Peng, X. Liu, Y. Liu, L. Zhao, G. Liu, X. Dong, J. Zhang, M. Nakatake, M. Arita, K. Shimada, H. Na-

- matame, M. Taniguchi, Z. Xu, C. Chen, X. Dai, Z. Fang, and X. J. Zhou, Evidence of topological surface state in three-dimensional Dirac semimetal Cd_3As_2 , [Sci. Rep. 4, 1 \(2014\)](#).
- [15] N. P. Armitage, E. J. Mele, and A. Vishwanath, Weyl and Dirac semimetals in three-dimensional solids, [Rev. Mod. Phys. 90, 015001 \(2018\)](#).
- [16] H. Weyl, Elektron und gravitation. i, [Z. Phys. 56, 330 \(1929\)](#).
- [17] A. A. Burkov and L. Balents, Weyl semimetal in a topological insulator multilayer, [Phys. Rev. Lett. 107, 127205 \(2011\)](#).
- [18] Z. Wang, H. Weng, Q. Wu, X. Dai, and Z. Fang, Three-dimensional Dirac semimetal and quantum transport in Cd_3As_2 , [Phys. Rev. B 88, 125427 \(2013\)](#).
- [19] S. Baidya and D. Vanderbilt, First-principles theory of the dirac semimetal Cd_3As_2 under Zeeman magnetic field, [Phys. Rev. B 102, 165115 \(2020\)](#).
- [20] T. Schumann, M. Goyal, H. Kim, and S. Stemmer, Molecular beam epitaxy of Cd_3As_2 on a III-V substrate, [APL Mater. 4, 126110 \(2016\)](#).
- [21] M. Uchida, Y. Nakazawa, S. Nishihaya, K. Akiba, M. Kriener, Y. Kozuka, A. Miyake, Y. Taguchi, M. Tokunaga, N. Nagaosa, Y. Tokura, and M. Kawasaki, Quantum Hall states observed in thin films of Dirac semimetal Cd_3As_2 , [Nat. Commun. 8, 1 \(2017\)](#).
- [22] Y. Liu, C. Zhang, X. Yuan, T. Lei, C. Wang, D. Di Sante, A. Narayan, L. He, S. Picozzi, S. Sanvito, R. Che, and F. Xiu, Gate-tunable quantum oscillations in ambipolar Cd_3As_2 thin films, [NPG Asia Mater. 7, e221 \(2015\)](#).
- [23] W. Yanez, Y. Ou, R. Xiao, J. Koo, J. T. Held, S. Ghosh, J. Rable, T. Pillsbury, E. G. Delgado, K. Yang, J. Chamorro, A. J. Grutter, P. Quarterman, A. Richardella, A. Sengupta, T. McQueen, J. A. Borchers, K. A. Mkhoyan, B. Yan, and N. Samarth, Spin and charge interconversion in dirac-semimetal thin films, [Phys. Rev. Applied 16, 054031 \(2021\)](#).
- [24] T. Schumann, L. Galletti, D. A. Kealhofer, H. Kim, M. Goyal, and S. Stemmer, Observation of the quantum Hall effect in confined films of the three-dimensional Dirac semimetal cd_3as_2 , [Phys. Rev. Lett. 120, 016801 \(2018\)](#).
- [25] L. Galletti, T. Schumann, D. A. Kealhofer, M. Goyal, and S. Stemmer, Absence of signatures of Weyl orbits in the thickness dependence of quantum transport in cadmium arsenide, [Phys. Rev. B 99, 201401\(R\) \(2019\)](#).

- [26] D. F. Liu, A. J. Liang, E. K. Liu, Q. N. Xu, Y. W. Li, C. Chen, D. Pei, W. J. Shi, S. K. Mo, P. Dudin, T. Kim, C. Cacho, G. Li, Y. Sun, L. X. Yang, Z. K. Liu, S. S. P. Parkin, C. Felser, and Y. L. Chen, Magnetic Weyl semimetal phase in a Kagomé crystal, [Science](#) **365**, 1282 (2019).
- [27] N. Morali, R. Batabyal, P. K. Nag, E. Liu, Q. Xu, Y. Sun, B. Yan, C. Felser, N. Avraham, and H. Beidenkopf, Fermi-arc diversity on surface terminations of the magnetic Weyl semimetal $\text{Co}_3\text{Sn}_2\text{S}_2$, [Science](#) **365**, 1286 (2019).
- [28] I. Belopolski, K. Manna, D. S. Sanchez, G. Chang, B. Ernst, J. Yin, S. S. Zhang, T. Cochran, N. Shumiya, H. Zheng, B. Singh, G. Bian, D. Multer, M. Litskevich, X. Zhou, S.-M. Huang, B. Wang, T.-R. Chang, S.-Y. Xu, A. Bansil, C. Felser, H. Lin, and M. Z. Hasan, Discovery of topological Weyl fermion lines and drumhead surface states in a room temperature magnet, [Science](#) **365**, 1278 (2019).
- [29] Y. Li and F. D. M. Haldane, Topological nodal Cooper pairing in doped Weyl metals, [Phys. Rev. Lett.](#) **120**, 067003 (2018).
- [30] Y. Liu, R. Tiwari, A. Narayan, Z. Jin, X. Yuan, C. Zhang, F. Chen, L. Li, Z. Xia, S. Sanvito, P. Zhou, and F. Xiu, Cr doping induced negative transverse magnetoresistance in Cd_3As_2 thin films, [Phys. Rev. B](#) **97**, 085303 (2018).
- [31] H. Wang, J. Ma, Q. Wei, and J. Zhao, Mn doping effects on the gate-tunable transport properties of Cd_3As_2 films epitaxied on GaAs, [Journal of Semiconductors](#) **41**, 072903 (2020).
- [32] S. A. Crooker, D. A. Tulchinsky, J. Levy, D. D. Awschalom, R. Garcia, and N. Samarth, Enhanced spin interactions in digital magnetic heterostructures, [Phys. Rev. Lett.](#) **75**, 505 (1995).
- [33] R. K. Kawakami, E. Johnston-Halperin, L. F. Chen, M. Hanson, N. Guébels, J. S. Speck, A. C. Gossard, and D. D. Awschalom, $(\text{Ga},\text{Mn})\text{As}$ as a digital ferromagnetic heterostructure, [Appl. Phys. Lett.](#) **77**, 2379 (2000).
- [34] A. I. Ril, I. V. Fedorchenko, S. F. Marenkin, A. V. Kochura, and A. E. Kuz'ko, Phase equilibria in the CdAs_2 – Cd_3As_2 – MnAs ternary system, [Russ. J. Inorg. Chem.](#) **62**, 976 (2017).
- [35] Y. Zhao, H. Liu, C. Zhang, H. Wang, J. Wang, Z. Lin, Y. Xing, H. Lu, J. Liu, Y. Wang, S. M. Brombosz, Z. Xiao, S. Jia, X. C. Xie, and J. Wang, Anisotropic Fermi surface and quantum limit transport in high mobility three-dimensional Dirac semimetal Cd_3As_2 , [Phys. Rev. X](#) **5**, 031037 (2015).

- [36] L. Galletti, T. Schumann, T. E. Mates, and S. Stemmer, Nitrogen surface passivation of the Dirac semimetal Cd_3As_2 , [Phys. Rev. Mater. **2**, 124202 \(2018\)](#).
- [37] P. Villar Arribi, J.-X. Zhu, T. Schumann, S. Stemmer, A. A. Burkov, and O. Heinonen, Topological surface states in strained Dirac semimetal thin films, [Phys. Rev. B **102**, 155141 \(2020\)](#).
- [38] Z. Wang, Y. Sun, X.-Q. Chen, C. Franchini, G. Xu, H. Weng, X. Dai, and Z. Fang, Dirac semimetal and topological phase transitions in A_3Bi ($\text{A} = \text{Na}, \text{K}, \text{Rb}$), [Phys. Rev. B **85**, 195320 \(2012\)](#).
- [39] S. M. Young, S. Zaheer, J. C. Teo, C. L. Kane, E. J. Mele, and A. M. Rappe, Dirac semimetal in three dimensions, [Phys. Rev. Lett. **108**, 140405 \(2012\)](#).

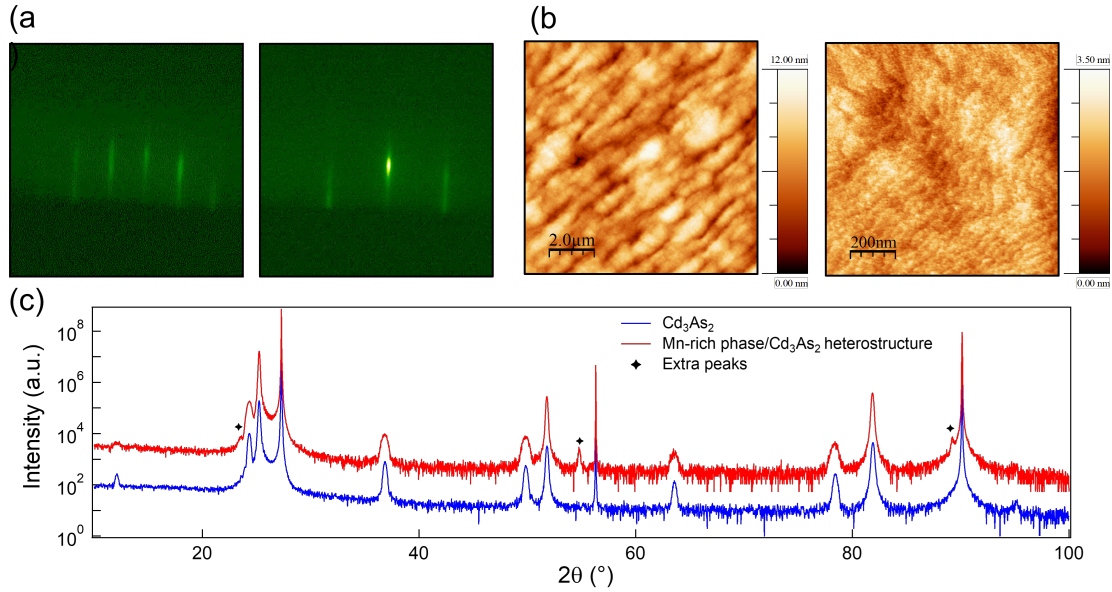


FIG. 1. (a) *In situ* RHEED patterns during MBE of a nominally 15 nm thick Mn-doped Cd_3As_2 heterostructure grown using the uniform doping approach. The electron beam is directed along $[0\bar{1}1]$ (left) and $[\bar{2}11]$ (right) direction. (b) *Ex situ* AFM images of the same sample as in panel (a). (c) Out-of-plane XRD of a nominally 25 nm thick Mn-doped Cd_3As_2 heterostructure grown using the uniform Mn-doping approach. The “extra peaks” in the XRD indicate the presence of a Mn-rich phase of unknown composition.

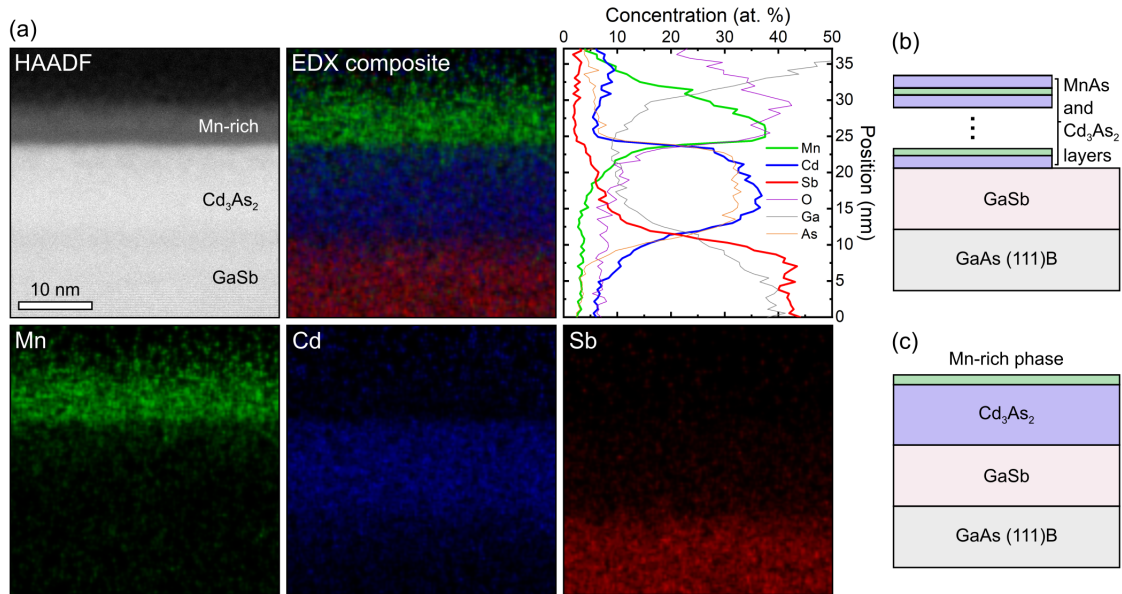


FIG. 2. (a) Low-magnification cross-sectional HAADF-STEM image of a Mn-rich phase/ Cd_3As_2 heterostructure that results from uniform Mn-doping during MBE growth of Cd_3As_2 . Composite and individual EDX maps show the spatial distribution of Mn, Cd, and Sb in the heterostructure as well as an atomic percent concentration profile across the heterostructure. Instead of being incorporated into the Cd_3As_2 lattice, a segregated Mn-rich phase formed on the top of the Cd_3As_2 layer. (b) Schematic of the delta doping method. (c) Schematic of the actual Mn-rich phase/ Cd_3As_2 heterostructure produced by the delta doping growth.

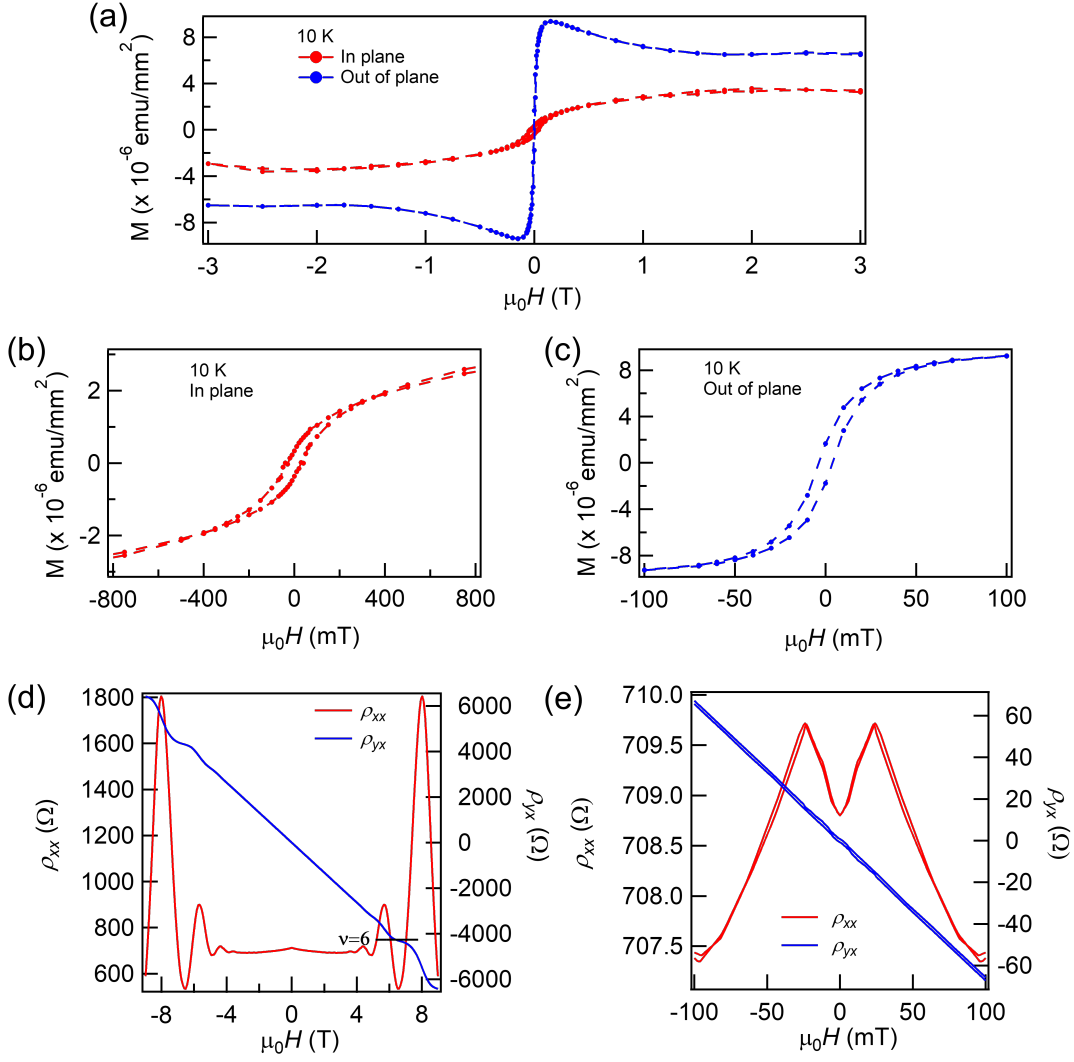


FIG. 3. Investigation of ferromagnetism in a Mn-rich layer/ Cd_3As_2 heterostructure. (a), (b), (c) SQUID magnetometry measurements of a 1 nm Mn-rich phase/ 7 nm Cd_3As_2 heterostructure at 10 K, respectively. The data suggest ferromagnetic ordering with an out-of-plane magnetic anisotropy. The inconsistency between the saturated magnetization values in the easy- and hard-axis measurements is an artifact created by the difficulty in properly handling the large filling factor when the thin film is mounted for field in plane measurements in the SQUID. (d) Observation of Shubnikov de Haas oscillations and an incipient integer quantum Hall effect in a 1 nm Mn-rich phase/ 7 nm Cd_3As_2 heterostructure at 2 K. (e) An expanded view of the low field magnetoresistance and Hall effect in panel (d).

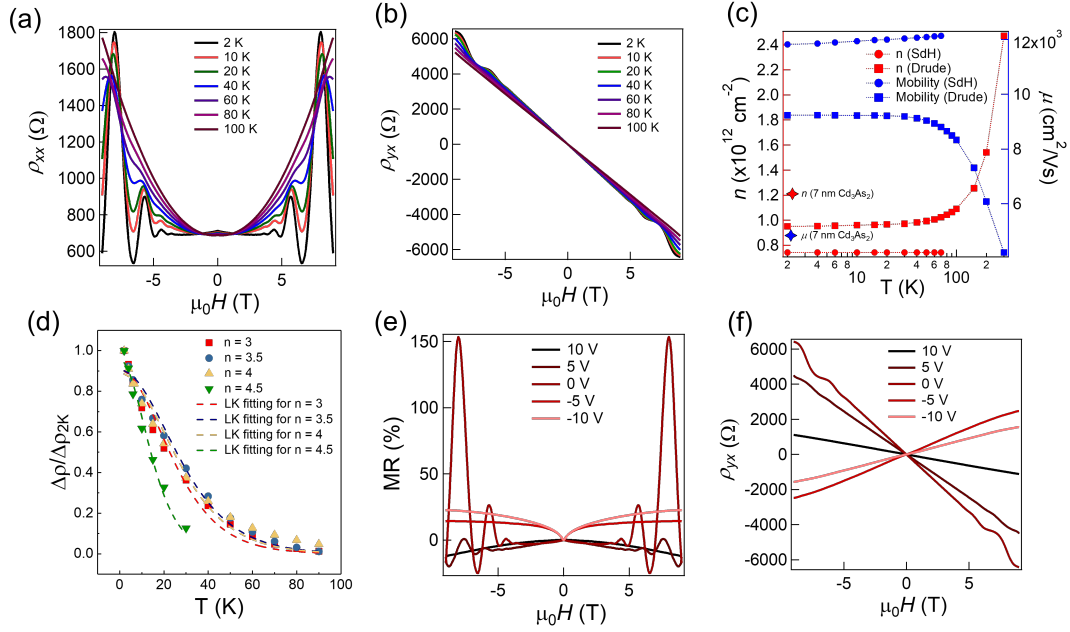


FIG. 4. Quantum oscillations in a 1 nm Mn-rich phase/ 7 nm Cd_3As_2 heterostructure. (a), (b) The temperature dependence of the quantum oscillations and Hall effect, respectively. (c) Temperature dependence of the carrier density and mobility. The values of the carrier density and mobility for a pristine Cd_3As_2 film of the same thickness are also shown at 2 K for comparison. (d) The fitting for the amplitude of the quantum oscillations at different filling factors with the Lifshitz-Kosevich formula. (e), (f) Gate dependence of the quantum oscillations and Hall effect, respectively.